

Article

Effects of Magmatic Fluids in Coals of São Pedro da Cova Coalfield, Douro Carboniferous Basin, Portugal: Insights from Inorganic Geochemistry

Mariana Costa ¹, Helena Moura ^{2,†}, Ary Pinto de Jesus ¹, Isabel Suárez-Ruiz ³ and Deolinda Flores ^{1,2,*}

¹ Departamento de Geociências, Ambiente e Ordenamento do Território, Faculdade de Ciências da Universidade do Porto, Rua do Campo Alegre, 687, 4169-007 Porto, Portugal; up201201358@edu.fc.up.pt (M.C.); adelmar@fc.up.pt (A.P.d.J.)

² Instituto de Ciências da Terra, Polo da Faculdade de Ciências da Universidade do Porto, Rua Campo Alegre 687, 4169-007 Porto, Portugal; helenaromoura@gmail.com

³ Instituto de Ciencia y Tecnología del Carbono (INCAR-CSIC), Francisco Pintado Fe 26, 33011 Oviedo, Spain; isruiz@incar.csic.es

* Correspondence: dflores@fc.up.pt

† 26 May 1991–16 May 2019.

Abstract: The Douro Carboniferous Basin (DCB), aged from Gzhelian, is an important coal-bearing basin occurring in Northern Portugal. While the coals and the sedimentary sequence of the DCB have been deeply studied, the inorganic geochemical data are scarce. This study intends to provide major and trace element contents and discuss their modes of occurrence and origins using a set of twenty-four coal samples from the São Pedro da Cova Coalfield taken from different sectors/outcrops. Thus, an integrated approach using petrographic, geochemical, both organic and inorganic, and mineralogical data was used to achieve these purposes. The main results demonstrated that these coals are anthracite A and vitrinite is the main organic component. Most of the elements have inorganic affinities and are associated with aluminosilicates, while the other elements have affinities with sulfides. Illite and muscovite are the main phyllosilicates occurring in these coals and pyrite is the most common sulfide. However, cinnabar, together with phosphates (fluorapatite, monazite, xenotime and gorceixite), were also identified. The enrichment of most elements as well as a heterogenous rare earth elements (REE) distribution pattern in the tectono-sedimentary unit (TSU) samples are related to magmatic fluids. On the other hand, on the Eastern Outcrop (EO), a tectonic slice, the subparallel trend of the REE distribution patterns, and a depletion of all the elements are related to the sedimentary contribution. The occurrence of cinnabar and gorceixite epigenetic mineralizations is interpreted as the action of a porphyry intrusion identified in this area of the DCB, between the TSU B1 and TSU D1.

Keywords: São Pedro da Cova Coalfield; organic petrology; trace elements; geochemical affinities; cinnabar; phosphates



Citation: Costa, M.; Moura, H.; Pinto de Jesus, A.; Suárez-Ruiz, I.; Flores, D. Effects of Magmatic Fluids in Coals of São Pedro da Cova Coalfield, Douro Carboniferous Basin, Portugal: Insights from Inorganic Geochemistry. *Minerals* **2022**, *12*, 275. <https://doi.org/10.3390/min12020275>

Academic Editors: Shifeng Dai and Davide Lenaz

Received: 28 November 2021

Accepted: 17 February 2022

Published: 21 February 2022

Publisher's Note: MDPI stays neutral with regard to jurisdictional claims in published maps and institutional affiliations.



Copyright: © 2022 by the authors. Licensee MDPI, Basel, Switzerland. This article is an open access article distributed under the terms and conditions of the Creative Commons Attribution (CC BY) license (<https://creativecommons.org/licenses/by/4.0/>).

1. Introduction

The São Pedro da Cova Coalfield is part of the Douro Carboniferous Basin (DCB), the most important coal-bearing basin in Portugal, and has been, since the early 1990s, the focus of several geological studies with emphasis on tectono-stratigraphic development, e.g., [1–5], paleobotany, e.g., [6–12], paleozoology, e.g., [6,7,13–16], organic petrology and physical parameters of the coals, e.g., [17–25], and coal exploration and its environmental impacts (e.g., [26–36]).

The coals of the DCB are anthracite A [22,25] and the coalification processes have been interpreted as due to the geothermal gradient increase promoted by granitic magmatism on the area as well as the regional geotectonic context [3,4,22]. The first geochemical data,

including only the content of some minor elements, was published by Lemos de Sousa [24], but the modes of occurrence of these elements were not identified being interpreted as corresponding to the inorganics associated with the organic matter. Furthermore, the influence of magmatic fluids in these coals was firstly reported by Moura et al. [37] and then by Costa et al. [38] based on geochemical data.

The minerals, as well as the elements occurring in the coals, are derived from the paleoenvironmental context where the organic matter was accumulated and from the modifications associated with the increasing rank as well as epigenetic processes, providing information on the depositional conditions and their post-depositional record. In general, the occurrence of igneous intrusions into coal-bearing sedimentary sequences is described in many basins of the world, e.g., [39–47], and is one of the events that can affect the properties of the organic and inorganic components of the coals. Thus, these magmatic events may be responsible for the coalification of coals, producing changes to its petrography, mineralogy and inorganic and organic geochemical composition.

The enrichment of elements, namely Hg [41,48–52] and REE, can also be due to the circulation of fluids of magmatic origin [53,54] and therefore associated to epigenetic mineralization. Although Hg occurs in coals in low abundance, it has been the focus of many studies due to its environmental concerns. According to Yudovich and Ketris [55], the Hg in coals is associated to clays, organic matter and sulfides. Normally, pyrite is the main carrier of Hg [56], but in coals extremely enriched in this element a Hg-sulfide, cinnabar, can occur [55].

In coals the P is mainly associated with phosphorus minerals occurring mainly as REE-phosphates (monazite, xenotime and crandallite group) and/or apatite [56]. Apatite and fluorapatite are the most common phosphorus-bearing minerals identified in coals; however, alumino-phosphates, namely minerals of the goyazite-gorceixite-crandallite-florencite group, can also be present ([57–59] and references therein). The source of P to promote the occurrence of these minerals can be the original peat biomass [57] but other origins can be pointed out as the occurrence of the goyazite-gorceixite minerals in coal seams can be an indicator of volcanic input ([59] and references therein). The occurrence of the goyazite-gorceixite minerals in coal seams as an indicator of volcanic input was initially reported by Goodarzi et al. [60], in tonsteins associated with bituminous coal of the East Kootenay Coalfields of British Columbia and also in coal-bearing strata in British Columbia [60,61].

In this study a multi-element geochemical study of the coal-bearing units of the DCB in the São Pedro da Cova Coalfield is presented and multi-proxy approach is taken: (i) to assess the affinities and mode of occurrence of the trace elements and the geological factors that may have controlled their origin and enrichment/depletion; and (ii) to identify the influence of the magmatic fluids on the inorganic fractions of the coal-bearing strata.

2. Geological Setting

In late- to post-orogenic time of the Variscan Orogeny the structured shear bands acquired a more brittle deformation, generating intermountain depressions which were filled by terrestrial sedimentation during the Pennsylvanian. One of those basins was the Douro-Beira Carboniferous Trough (DBCT) where the DCB fills part of a pull-apart basin in the Central Iberian Zone (CIZ) of the Iberian Massif, that is aligned along a major brittle shear band, the Douro-Beira Shear Zone (DBSZ). The São Pedro da Cova Coalfield is part of the DCB. The main geological context is depicted in Figure 1. The Douro Carboniferous Basin was dated from the Gzhelian (lower Stephanian C) based on its flora (herein [8–12]) and fauna, e.g., [6,7,13,14].

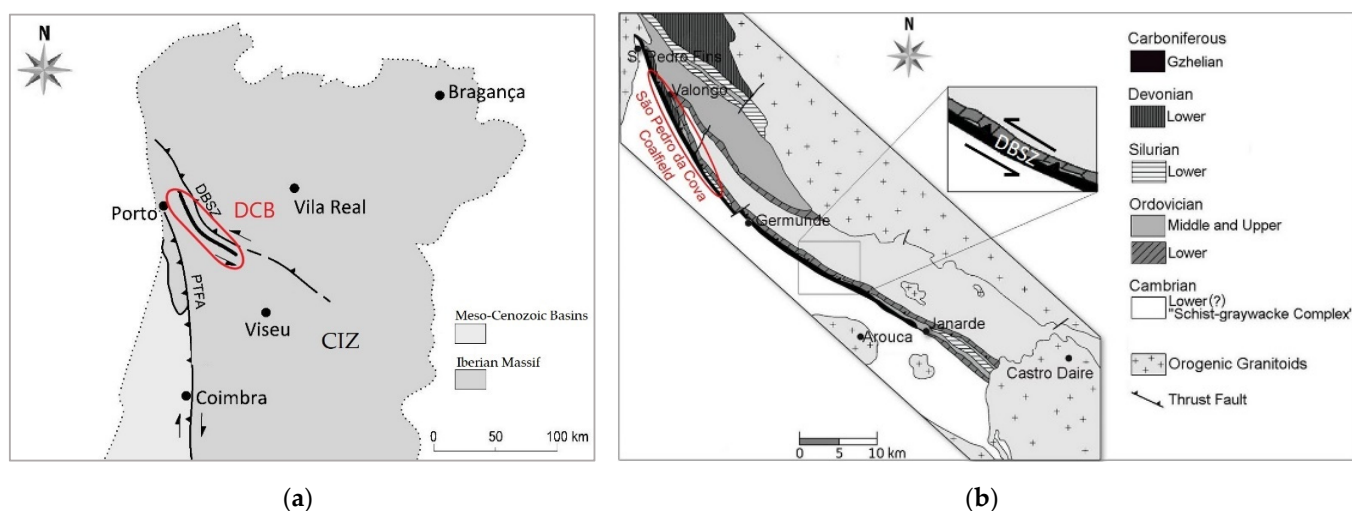


Figure 1. Simplified geological setting of DCB: (a) location of DCB in the CIZ of the Iberian Massif; (b) main geological setting of São Pedro da Cova Coalfield in the DCB and relation with DBSZ (modified with permission from ref. [5], Copyright 2019 Springer Nature Switzerland AG).

The coal exploitation in the DCB is reported from the end of XVIII century, beginning at the São Pedro da Cova Coalfield. This exploitation was responsible for intense coal mining in several underground and open mines of two coalfields (São Pedro da Cova and Pejão Coalfields) especially during periods of world wars.

According to Pinto de Jesus [5], the DBCT was generated as a pull-apart basin related with left transtensional tectonics that occurred in two major and similar episodes at different times. The first one took place during the Moscovian (Westphalian) in relation to the third phase (D3) of the Variscan Orogeny. The second, and stronger episode, occurred during the lower Gzhelian (lower Stephanian C) in relation to the late phases of the Variscan Orogeny. The tectonic reactivation of the sinistral transcurrent shear in the DBCT formed another pull-apart basin with a gradually migrating depocenter from NW to SE to the area south-eastward of Germunde. In the São Pedro da Cova sector (NW part of the DCB), the opening by pull-apart promoted the crustal thinning which led to limited volcanism, as indicated by eruptive materials recognized underground interbedded with coal seams in the São Pedro da Cova Coalfield [62,63]. Teixeira and Fonseca [62] reported the occurrence of a vein of an eruptive rock between the TSU B1 and TSU D1. In the same year, Pereira [63] carried out a petrographic study of these rocks, agreeing with its vein nature and classified them as granodioritic porphyry, distinguishing two different formations, a leucocratic granodioritic porphyry, of greenish tonality, and a dark granodioritic porphyry, posterior to the first.

The base of the DCB rests unconformably over the “Schist-graywacke Complex” (lower Cambrian?) along most of the basin except at Sete Casais outcrop (NW sector) where the basal contact is made by angular discordance over the terrestrial Moscovian from the Bougado-Ervedosa Basin [5,64]. The strip is thrust by the reverse limb of the Valongo anticline. Despite the strong tectonic deformation, a lithological succession was erected together with the composing lithofacies, which constitute the Germunde Formation [5]. The Germunde Formation, after the sequence established by Pinto de Jesus [3,4] (Figure 2), is composed of four main tectono-sedimentary units (TSU, in sense of Megias [65]) with a total thickness of circa 350 m.

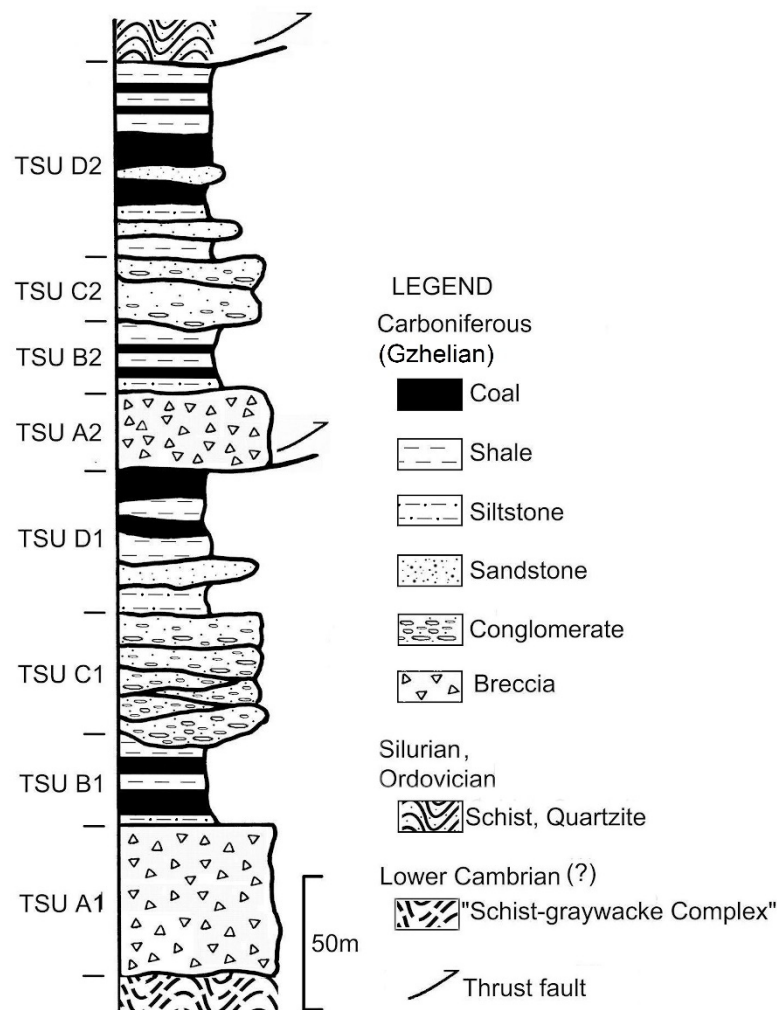


Figure 2. Synthetic lithological succession of the Germunde Formation of the DCB [5]. TSU A—Debris-flow dominated alluvial fan characterized by matrix-supported breccia; TSU B—Lacustrine/palustrine system marked by fossiliferous shales and coal seams; TSU C—Braided fluvial complex developing multi-story/multichannel architecture with predominant SE to NW paleocurrent flow and minor lateral flows from tributaries; TSU D—Lacustrine or palustrine system formed by fossiliferous shale beds and coal seams with intercalations of sandy-conglomeratic beds of deltaic lobes whose main flows had its source in the NE margin, the rock clasts being mainly composed by quartzite, schist, and lydite (black chert) with provenance from Ordovician and Silurian terranes. The succession is repeated by a thrust fault, the reason by which the unit's symbols are marked by the numbers 1 and 2 (modified with permission from ref. [5], Copyright 2019 Springer Nature Switzerland AG).

The lithological succession is segmented in tectonic slices controlled by thrust faults which form a triplex in the São Pedro da Cova region (Figure 3). The eastern tectonic slice of the Gzhelian of the DCB has come to be traditionally designated as the "eastern basin". As it is part of the DCB instead of being a different basin, this structure will now be designated as Eastern Outcrop (EO) and should also be designated as such in the future.

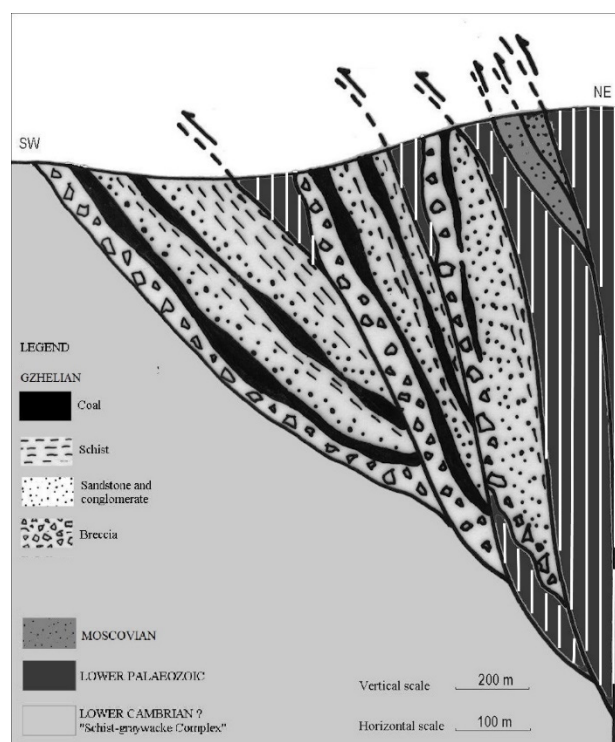


Figure 3. Synthetic tectonic structure of the DCB at São Pedro da Cova Coalfield (after [3]).

Regarding the coalification of the coals of this coal-bearing sedimentary section, considering the sedimentological record, the structural deformation and evolution, and also the data obtained by Lemos de Sousa [22] and Pinto de Jesus [3,4], two main episodes of coalification are suggested, both in good relationship with the later- to post-orogenic granitic magmatism. The first episode occurred before the tilting and the tectonic slicing of the basin. The other one, stronger than the first, took place after the tilting of the basin, and was contemporaneous of the thrust faulting that sliced the DCB.

3. Sampling and Analytical Methodologies

For this study, twenty-four coal representative channel samples were selected, namely: four samples from TSU B1; and five samples from each of the TSU D1, TSU B2, TSU D2 and EO units for petrographic, geochemical, both organic and inorganic, and mineralogical studies. In the Table S1 it is included the identification of the samples and their localization (see also Figure 4) and in the Table S2 the analytical data obtained in the studied samples are provided.

The petrographic analysis included maceral composition and vitrinite random reflectance, which were carried out following standard procedures ([66,67], respectively), using polished blocks prepared according to ISO 7404-2 [68]. They were analyzed using a Leica DM4000 microscope fitted with “Discus-Fossil” software. The ICCP 1994 System nomenclature was used for the identification of organic particles [69,70].

Proximate analysis was carried out under standardized conditions [71–73] and ultimate analysis was performed using a LECO CHN-2000 (LECO Corporation, St. Joseph, MI, USA) for C, H, N and a LECO S632 (LECO Corporation, St. Joseph, MI, USA) for total S (S tot). Results were obtained on a dry basis (% d) and then volatile matter (VM), C, H, and N were calculated on a dry and ash-free basis (% daf) in accordance with ISO 1170 [74].

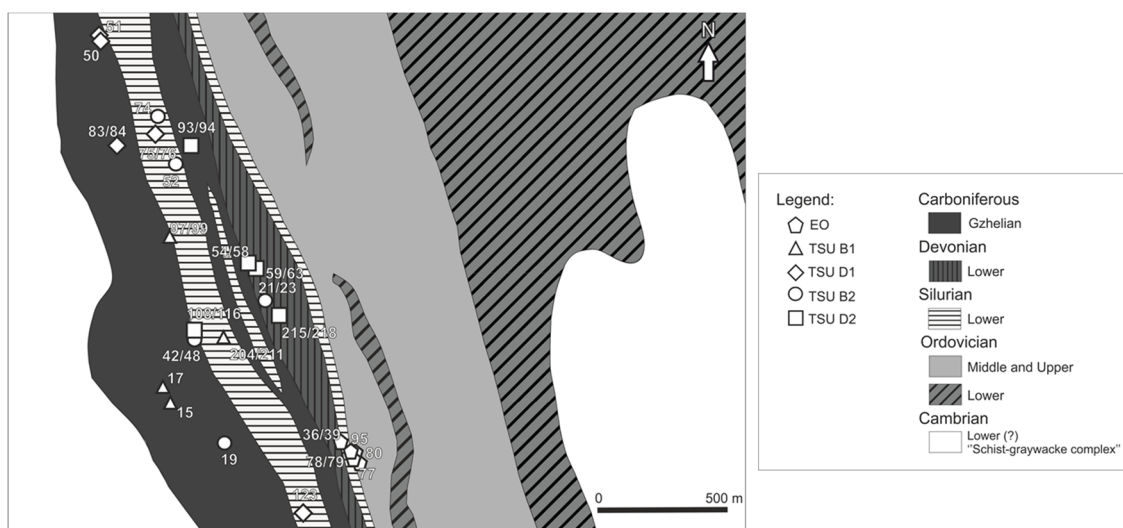


Figure 4. Location of the studied samples (see also Figure 1 for more details in the geographical localization).

Major and trace element composition of the studied samples (including Hg) were determined by inductively coupled plasma-optical emission spectrometry (ICP-OES) and by inductively coupled plasma-mass spectrometry (ICP-MS) at the Acme Analytical Laboratories (Canada). The major elements, Ba and Sc concentrations were obtained using ICP-OES, with a Spectro Ciros/Arcos instrument, and following lithium metaborate/tetraborate fusion dissolved in nitric acid (ACS grade). The same fusion procedure was used for the following elements Be, V, Co, Ga, Rb, Sr, Y, Zr, Nb, Sn, Cs, Hf, Ta, W, Th, U and REE, but their concentration was obtained using ICP-MS (ELAN 9000, PerkinElmer, Inc., Waltham, MA, USA). The other elements (Ni, Cu, Zn, As, Se, Mo, Ag, Cd, Sb, Au, Hg, Tl, Pb and Bi) were analyzed, after an Aqua Regia digestion (1:1:1 HNO₃:HCl:H₂O), using ICP-OES/MS. Internal standard, SO-19, was used for quality check of lithium fusion procedure analysis, and Certified Reference Materials (DS11 and OREAS262) for Aqua Regia digestion analyses. Analysis of blanks and duplicates with analytical error <1% were used to calibrate the analytical results.

Scanning Electron Microscopy with Energy Dispersive Spectroscopy (SEM-EDS) analyses were performed using a high-resolution (Schottky) environmental scanning electron microscope (ESEM) fitted with an X-Ray microanalysis and electron backscattered diffraction analysis device Quanta 400 FEG ESEM/EDAX Genesis X4M (FEI company, Hillsboro, OR, USA). The analyses were carried out on polished blocks of selected samples coated with a thin film of C, by vapor deposition, using JEOL JEE—4X Vacuum Evaporator equipment (JEOL, Tokyo, Japan) at the Materials Center of the University of Porto (CEMUP).

4. Results and Discussion

4.1. Organic Petrography and Ultimate and Proximate Analyses

The results of the petrographic analysis are reported in Table S2. In these samples it can be observed that the vitrinite reflectance varies between 4.51% and 5.76%, classifying these coals, according to ISO 11760 [75], as anthracite A. These results agree with previously published data [22,25]. Figures 5 and 6 show some relevant petrographic aspects of these coals. The maceral composition, which is reported in percentage by volume and minerals-free-basis, shows that vitrinite is the predominant maceral group corresponding to more than 90% of the samples. The subgroup with the highest expression is that of telovitrinite (38 vol.% to 95 vol.%, Figure 5A–D and Figure 6B–D), followed by detrovitrinite (2 vol.% to 51 vol.%, Figures 5B and 6A). The gelovitrinite subgroup is scarce (<1 vol.%). The inertinite group ranges between 1 vol.% and 11 vol.%, with semifusinite (1 vol.% to 10 vol.%, Figure 5B) being the most abundant maceral

followed by fusinite (<1 vol.% to 2 vol.%, Figure 5C), and inertodetrinite (1 vol.%) and macrinite (<1 vol.%) were sporadically observed.

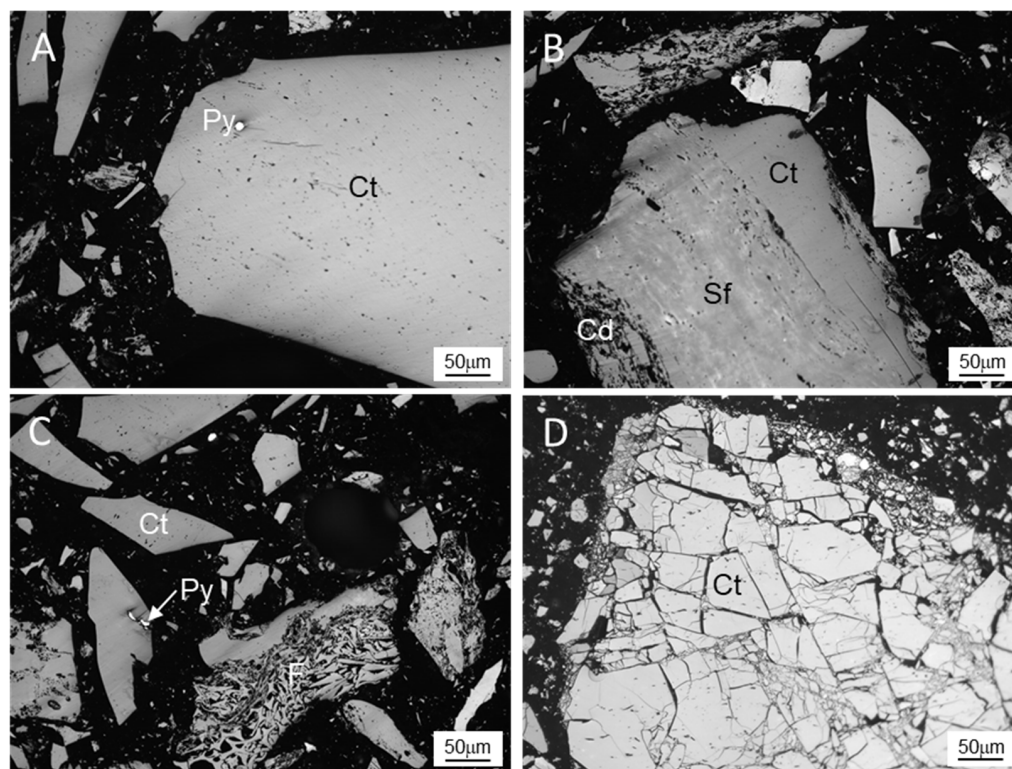


Figure 5. Photomicrographs of the studied coals. (A) Collotelinite (Ct) and framboidal pyrite (Py); (B) collotelinite (Ct), collodetrinite (Cd) and semifusinite (Sf); (C) collotelinite (Ct), fusinite (F) and epigenetic pyrite filling a fracture in the collotelinite; (D) collotelinite (Ct) mylonitized. Photomicrographs taken under reflected white light (A–C sample 95 from TSU B1; D sample 77 from EO).

The minerals content ranges from 0 vol.% to 9.8 vol.%, which mostly includes quartz, pyrite, carbonates and clays (Figure 5A,C and Figure 6A–D). Framboidal pyrite is syngenetic (Figure 5A) while the pyrite that is filling fractures in the collotelinite is epigenetic (Figures 5C and 6B). Regarding the carbonates (Figure 6C,D), the growth within the organic matter in the form of concretions indicates that they are syngenetic [76].

The proximate and ultimate analysis data are reported in Table S2. The ash yield, expressed on a dry basis, presents a high range of values corresponding from low to high ash yield (4.86% to 39.72%). The volatile matter content (dry ash-free basis) is low, ranging from 3.99% to 14.90%. The ultimate analysis data, reported on a dry ash-free basis, indicate a high C content (83.62% to 95.61%) and low values in H (1% to 2.24%), N (0.92% to 1.53%) and O (0.44% to 9.35%). These data (C, H, VM) agree with the rank of these coals. The S tot contents are low and do not vary much in the studied samples (0.44% to 1.83%). However, sample 15 is the one that stands out from all the others, with 3.36%.

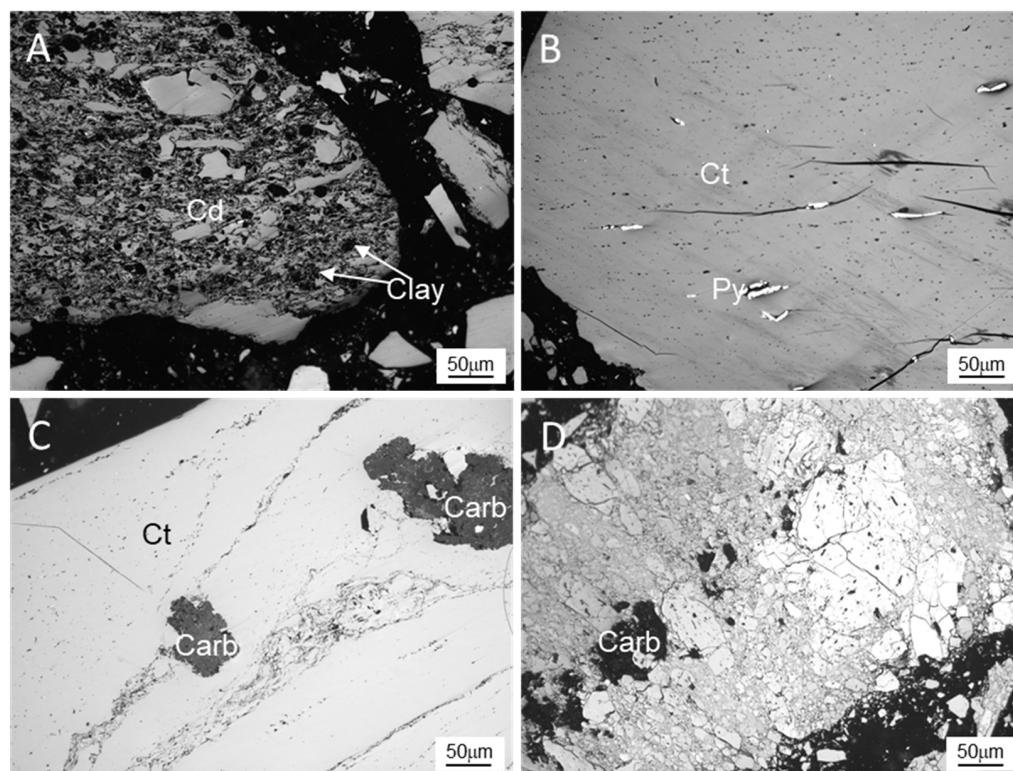


Figure 6. Photomicrographs of the studied coals. (A) Collodetrinite (Cd) and clay minerals (clay); (B) epigenetic pyrite (Py) filling a fracture in the collotelinite (Ct); (C) carbonates in the collotelinite (Ct); (D) carbonates in the collotelinite (Ct) mylonitized. Photomicrographs taken under reflected white light (A–C sample 15 from TSU B1; D sample 77 from EO).

4.2. Major Elements and Mineralogy

The major and trace element compositions of the studied samples are shown in Table S2. The contents of major elements agree with the mineralogy identified in these samples. Thus, the Al contents are higher than those of Si, evidencing the presence of clay minerals (Figures 6A, 7 and 8), but quartz is also present. The clay minerals present in these samples are detrital (Figures 6A and 7), but in some cases an authigenic origin can be pointed out as they are filling cellular vacuoles (Figure 8). Potassium is associated with phyllosilicates, namely illite, but epigenetic muscovite was also identified (Figure 9). The Fe content is due to the presence of pyrite which, as mentioned before, occurs either as syngenetic framboids (Figure 5A) or filling fractures in the organic matter (Figures 5C and 6B) and are therefore epigenetic. Other sulfides were identified in the studied samples (Figure 10), such as: galena (Pb), sphalerite (Zn) and chalcopyrite (Cu and Fe). Calcium is associated with carbonates, as ankerite was identified in some samples as well as fluorapatite (Figures 9 and 11). The P occurs associated with phosphates that in the samples of this sector of the basin occur with a diversified composition and, in some cases, with the presence of REE. The most common phosphate is fluorapatite (Figures 9 and 11) which sometimes has an epigenetic origin (Figure 9), but xenotime (Y phosphate, which frequently contains Dy and Gd, Figure 7), monazite (Ce phosphate with La and Nd, Figure 8) and gorceixite (Ba aluminophosphate, Figure 12) were also identified. Titanium oxides, such as rutile or anatase, and zircon are present and associated with both quartz and clays. Barite, a Ca sulfate (Figure 11), was also observed.

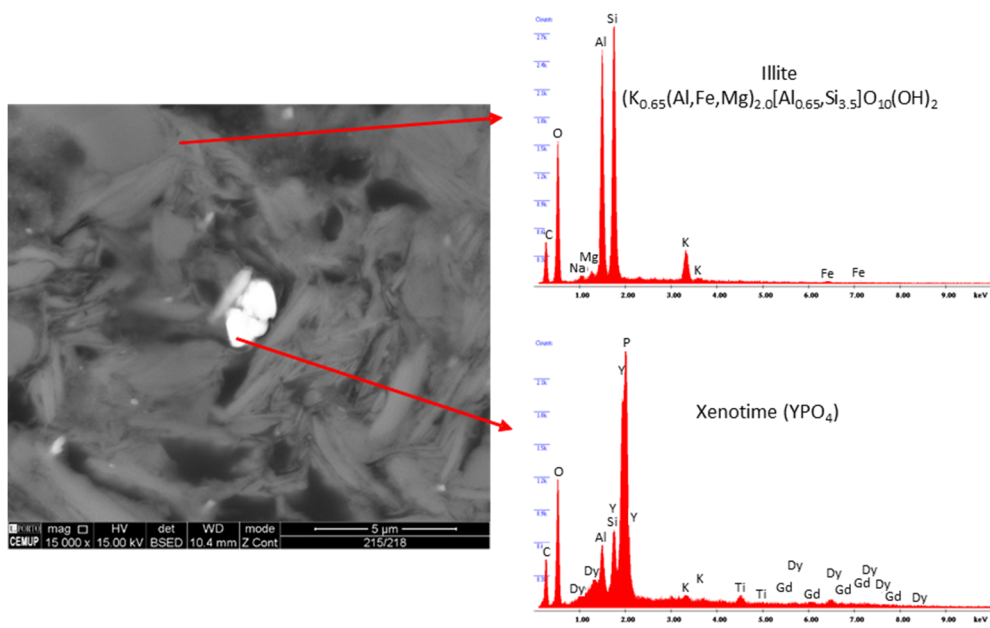


Figure 7. SEM (BSE images) and EDS spectrum of the mineral phases in the coals: illite and xenotime (sample 215/218 from TSU D2).

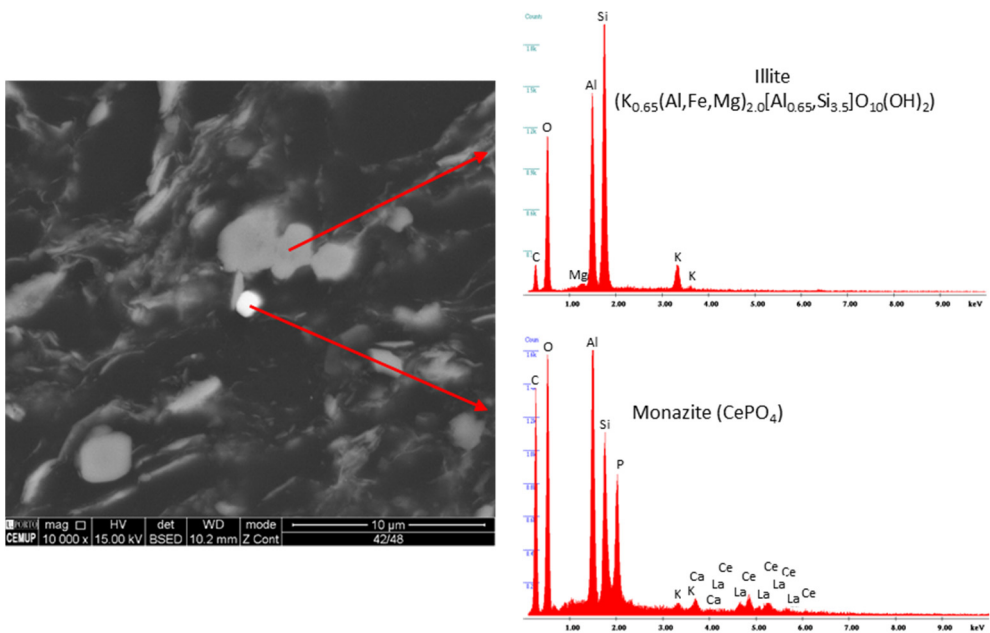


Figure 8. SEM (BSE images) and EDS spectrum of the mineral phases in the coals: illite and monazite (sample 42/48 from TSU B2).

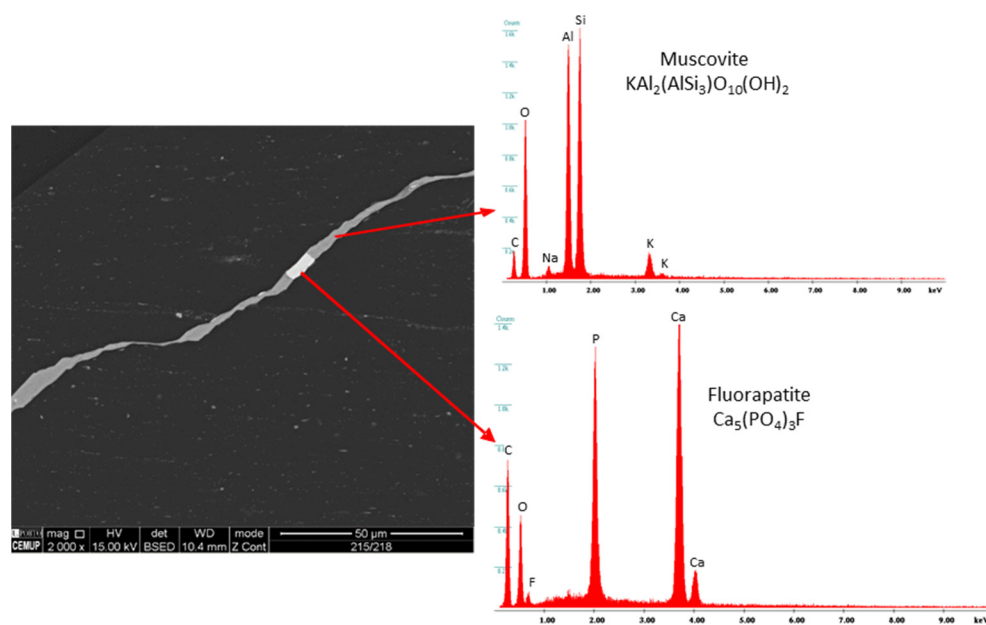


Figure 9. SEM (BSE images) and EDS spectrum of the mineral phases in the coals: muscovite and fluorapatite (sample 215/218 from TSU D2).

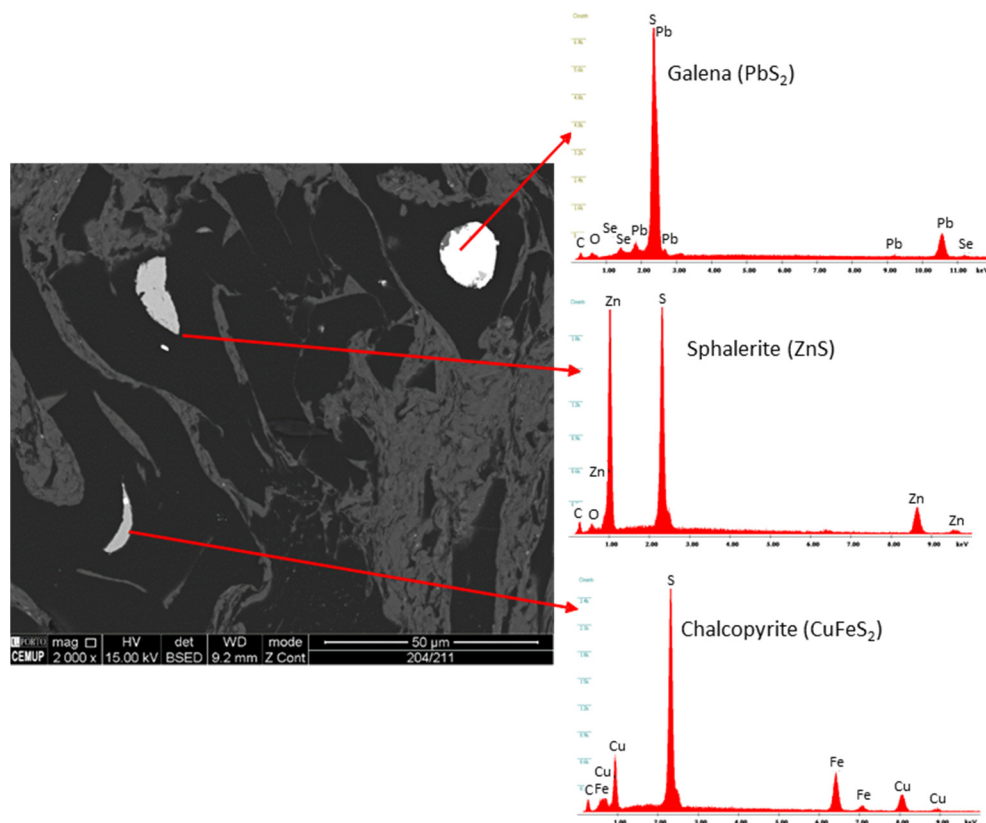


Figure 10. SEM (BSE images) and EDS spectrum of the mineral phases in the coals: galena, sphalerite and chalcopyrite (sample 204/211 from TSU B1).

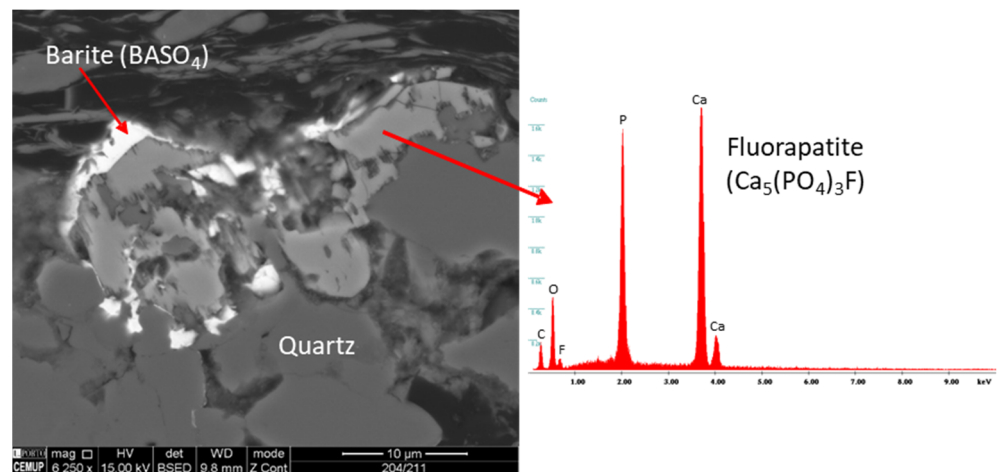


Figure 11. SEM (BSE images) and EDS spectrum of the fluorapatite in the coals. Barite and quartz were also identified (sample 204/211 from TSU B1).

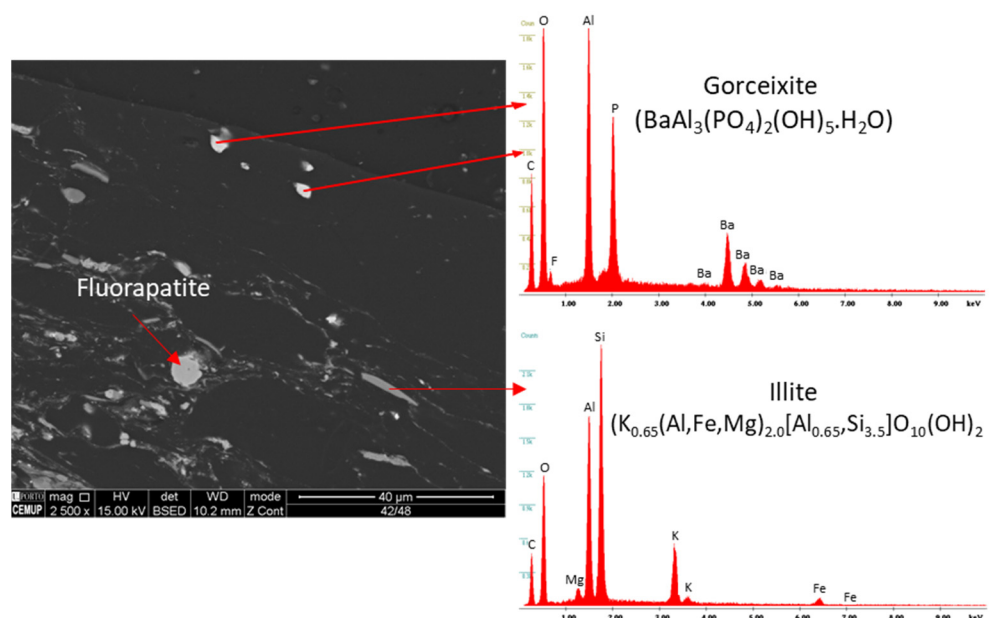


Figure 12. SEM (BSE images) and EDS spectrum of the mineral phases in the coals: gorceixite and illite. Fluorapatite was also identified (sample 42/48 from TSU B2).

4.3. Trace Elements and Concentration Coefficients

The concentration coefficients (CC) were calculated through the ratio between the concentration of the element in each of the studied samples and the respective reference average values of trace element concentrations in the world's hard coals proposed by Ketrís and Yudovich [77], and then classified according to Dai et al. [78,79] as follows: depleted ($CC < 0.5$), normal ($0.5 < CC < 2$), slightly enriched ($2 < CC < 5$), enriched ($5 < CC < 10$), significantly enriched ($10 < CC < 100$) and extremely enriched ($CC > 100$). The CCs of all studied samples are plotted in Figures 13 and 14.

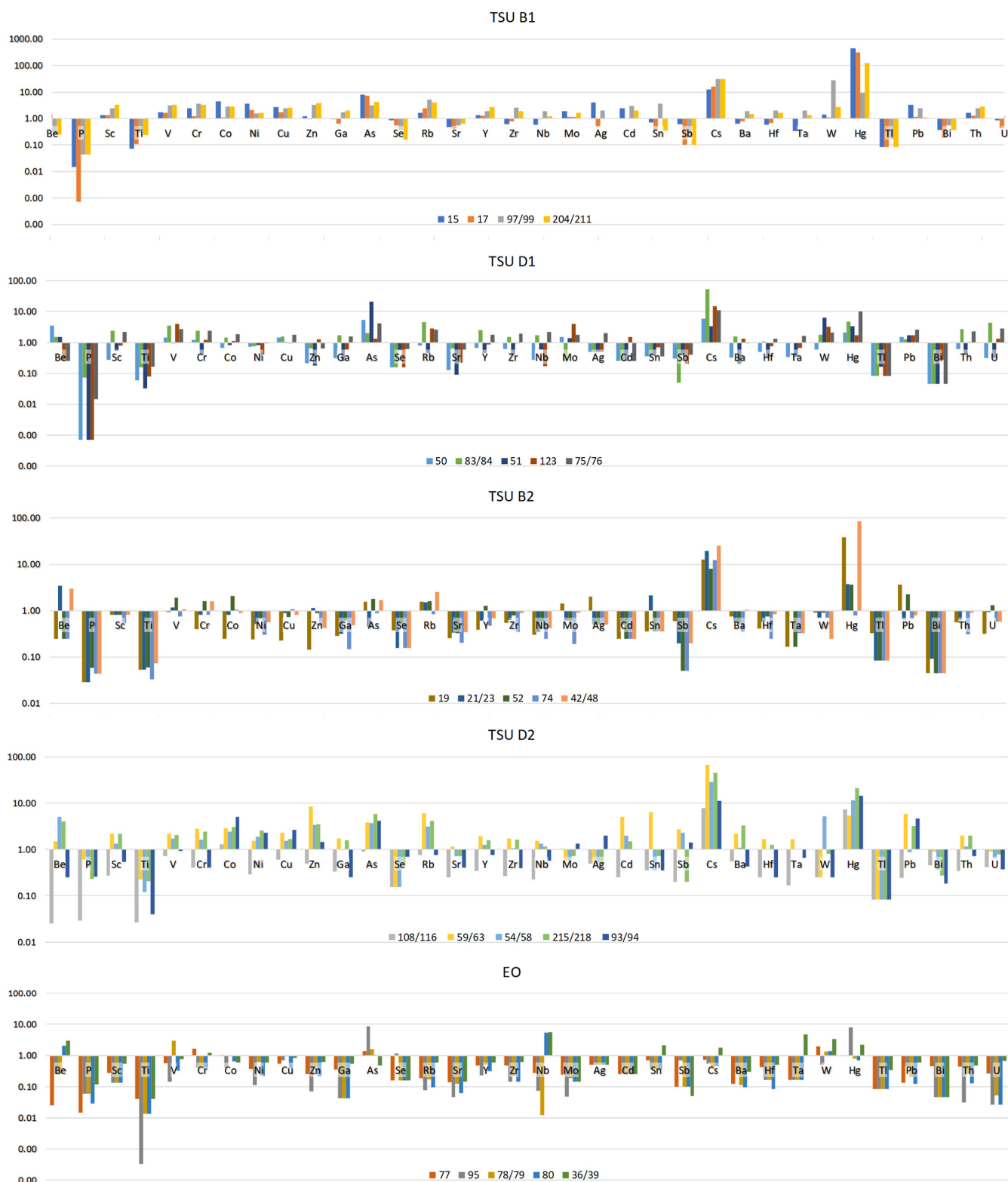


Figure 13. Concentration coefficients (CC) of trace elements for the studied samples from TSU and EO, normalized by average trace element concentrations in the world hard coals [77].



Figure 14. Concentration coefficients (CC) of REE for the studied samples from TSU and EO, normalized by average trace element concentrations in the world hard coals [77].

The CCs of the TSU B1 samples show that Hg is extremely enriched, and cinnabar, a Hg sulfide, was identified (Figure 15); Cs enrichment is quite evident in all samples (CC > 10). Arsenic and W are considered enriched; however, it is observed that sample 97/99 is the one that presents a rather significant enrichment on this last element. Elements such as Cd, Co, Cr and Zn are slightly enriched, except for sample 17 that has a normal content of these elements. Cu, Ni, Rb, Sc, Th, V and the LREE also present a slight enrichment in all samples. The elements

with normal CC are Ag, Ba, Be, Ga, Hf, Mo, Nb, Pb, Sn, Sr, Ta, U, Y, Zr and the HREE. However, Be stands out from this group as it shows a general depletion in all samples, especially in sample 15, while sample 17 shows a small enrichment. The elements P, Ti, Bi, Sb, Se and Tl present a clear depletion in all samples of this unit.

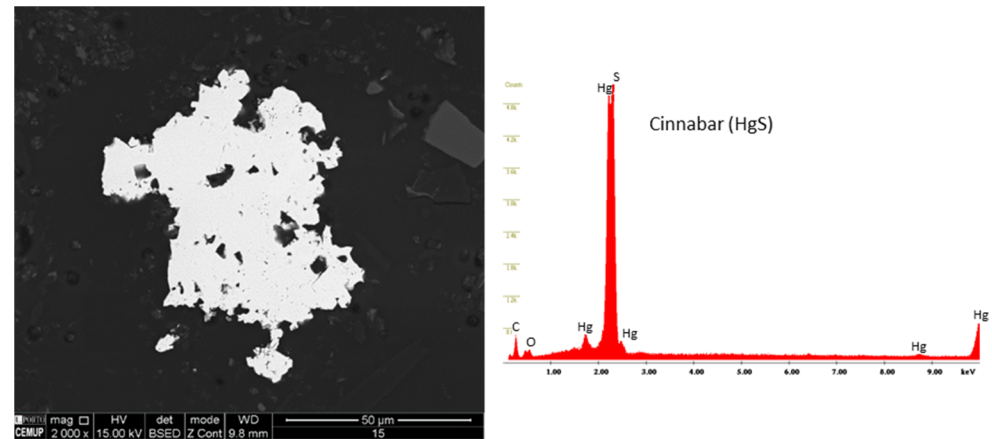


Figure 15. SEM (BSE images) and EDS spectrum of the cinnabar identified in the studied coals (sample 15 from TSU B1).

In the TSU D1 enrichments in As, Cs and Hg are evident in all samples, although only slightly. Elements such as Rb, V and W are also classified as slightly enriched; however, sample 50 is slightly depleted in Rb and W, and sample 51 in Rb and V. The elements with a normal CC value are Ag, Ba, Be, Co, Cr, Cu, Ga, Hf, Mo, Nb, Ni, Pb, Sc, Ta, Th, U, Y, Zn, Zr and the REE. It should be noted that samples 83/84 and 75/76 show an enrichment in all REE except Tm, while all other samples show depletion in these elements. Phosphorus, Ti, Bi, Sb, Se and Tl are elements quite depleted in all samples.

The CCs relating to the TSU B2 samples show a high enrichment in Cs and in Hg in all samples, except for sample 74, which shows a slight depletion in Hg. The elements Ag, As, Ba, Be, Co, Cr, Cu, Hf, Mo, Pb, Rb, Sc, Sn, Th, U, V, W, Y, Zn, Zr and the LREE show a normal CC, but with an apparent tendency to depletion, exhibiting in some cases slight enrichment to counteract this tendency. On the other hand, P, Ti, Bi, Cd, Ga, Nb, Ni, Sb, Se, Sr, Ta, Tl and the HREE present a clear depletion in all samples.

As in the TSU B2, in the TSU D2 the most significant enrichments in all samples are in Cs and Hg. Cobalt shows slight enrichments as well as As and Zn except for sample 108/116. Beryllium, Pb and Rb also present slight enrichments. The elements Ag, Ba, Cd, Cr, Cu, Ga, Hf, Mo, Nb, Ni, Sb, Sc, Sn, Sr, Ta, Th, U, V, W, Y, Zr and all REE, except Tm, show normal CC, whereas P, Ti, Bi, Se, Tl, Tm are elements with clear depletion in all samples.

The CC of the EO show a general depletion in all elements, except for As, Hg, Nb, Be, Co, Cr, Cs, Cu, Sn, Ta, V, W that show a normal to slightly enrichment in some samples.

4.4. Geochemical Affinities of the Trace Elements

Pearson correlation coefficients were calculated and used to determine the geochemical affinities of the elements. The correlations between the elements and the ash yield were used to identify the organic and/or inorganic affinities of the elements, as follows: organic affinities ($r_{\text{ash}} < -0.5$), intermediate affinities ($-0.5 < r_{\text{ash}} < +0.5$) and inorganic affinities ($r_{\text{ash}} > +0.5$). Affinities with aluminosilicates ($r_{\text{Al-Si}} > 0.50$) and with sulfur ($r_{\text{S tot}} > 0.50$) were also identified. To complement this statistical analysis, a hierarchical cluster classification analysis was also performed for all TSU as well as for the EO.

In the TSU B1 the elements S, As, Hg, Ni and Se present an organic affinity; Fe, Ag, Be, Cd, Co, Cu, Mo, Pb, Sb and Sn, Tl intermediate affinities; and, Al, Si, Ca, Mg, K, Na, P, Ti, Ag, Co, Cr, Cs, Cu, Ga, Hf, Hg, Nb, Ni, Rb, Sc, Sr, Ta, Th, U, Y, Zr, La, Ce, Pr, Nd, Sm, Eu, Gd, Tb, Dy, Ho, Er, Tm, Yb and Lu, inorganic affinities. The elements with an affinity for aluminosilicates also have inorganic affinities, except for Tl, which

has an intermediate affinity. The elements with affinities for sulfur are Ag, Hg, Ni, Pb, Sb and Se. The dendrogram of this unit (Figure 16) shows two main groups, one associated with aluminosilicates, where REE are included. The other association includes sulfur and elements associated with the sulfides identified in these samples, such as Fe, Hg, Cu, Zn and Pb. Phosphorous is also in this group associated with Ca which coincides with the presence of fluorapatite. Note also that the Cs, Rb and K association is clear in the group of the aluminosilicates, which may be responsible for the enrichment of Cs, and also Rb, in both the illite (Figures 7, 8 and 12) and muscovite (Figure 9) identified in these samples. The geochemical association of Cs with K and Rb is suggested by Finkelman et al. [80].

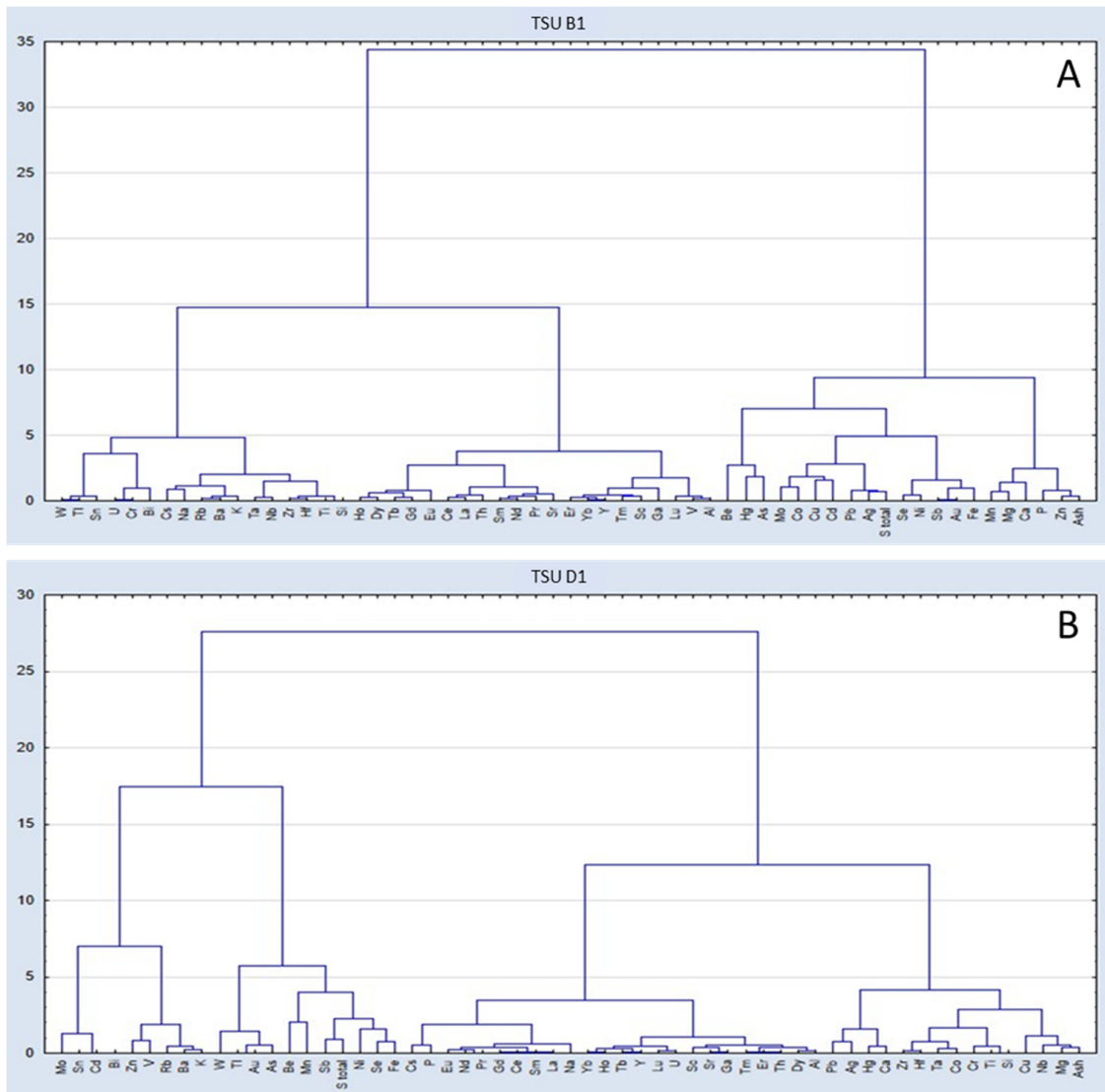


Figure 15. Cont.

Ho, Er, Tm, Yb and Lu have inorganic affinities, which, such in TSU B1, include all the elements with aluminosilicate affinities, except Ba, which is included in the elements with intermediate affinities.

The elements with affinities to sulfur are Fe, As and Sb, which may result from the presence of pyrite and chalcopyrite, whereas Sb may be due to the presence of antimony mineralization recognized in this area and described as pre-concentrated in the breccia from TSU A1 (see Figure 2) as referred by Couto [81]. Therefore, and observing the dendrogram corresponding to this unit (Figure 16), it is once again distinguishable two main groups, one corresponding to the organic affinities, which also coincide with the affinities for sulfur, while the other corresponds to the elements of inorganic affinities, coinciding with the affinities of aluminosilicates, where the REE are included. In this unit P is in the aluminosilicates group, occurring in the form of phosphates dispersed in the clay minerals.

In the TSU B2, the elements with organic affinities are Fe, As and Sb, while the elements Si, Mg, Fe, Mn, Ti, As, Ba, Be, Bi, Cd, Cs, Hg, Mo, Pb, Rb, Sc, Se, Sn, Ta, W and Zn have intermediate affinities. The elements with inorganic affinities are Al, Ca, K, Na, P, Co, Cr, Cu, Ga, Hf, Nb, Ni, Sr, Th, U, V, Y, Zr, La, Ce, Pr, Nd, Sm, Eu, Gd, Tb, Dy, Ho, Er, Tm, Yb and Lu. The elements with affinities for aluminosilicates correspond only to K, Ti, Cr, Ga, Hf, Nb, Ni, Sc, Sr, Th, Zr, Tm, Yb and Lu, which correspond mostly to the elements with inorganic affinities, Ti and Sc being the exceptions as they have intermediate affinities. Concerning the affinities with sulfur, only the elements Ag, Mo, Pb, Sb and Tl evidence this association, which is slightly different in comparison with the previous described units. In the dendrogram of this unit (Figure 16), two groups are again distinguished, now one that corresponds to the group essentially of the REE, which includes P, coinciding with the presence of phosphates with REE being the group of inorganic affinities. The other group comprises the elements with organic and intermediate affinities, where the elements with sulfur affinities are also included.

The TSU D2, the one on the top of the sequence (see Figure 2), only has S and Mo as elements with organic affinities, and the elements Mg, Ag, Au, Bi, Co, Cu, Hg, Pb, Se and W with intermediate affinities. The remaining elements (Ca, Mg, K, Na, P, Ti, As, Ba, Be, Cd, Cr, Cs, Ga, Hf, Nb, Pb, Rb, Sc, Sn, Sr, Ta, Th, U, V, Y, Zn, Zr, La, Ce, Pr, Nd, Sm, Eu, Gd, Tb, Dy, Ho, Er, Tm, Yb, Lu) have inorganic affinities, being similar to the first two units. As in TSU B1 and TSU D1, the elements with affinities to aluminosilicates have inorganic affinities, except for Pb, which has an intermediate affinity. The elements with affinity to sulfur are Ag, Co, Cu, Mo and Se. Once again, the dendrogram obtained for the TSU D2 (Figure 16) is divided into two main groups, the first one corresponding to the elements with organic and intermediate affinities, and a second one corresponding to the aluminosilicates where the REE present in the phosphates are dispersed in the clay minerals.

The EO stands out from the other units, as the elements Mn, S, As, Sb and Se have organic affinities and the elements Ca, Fe, Na, Au, Ba, Bi, Co, Cu, Hg, Mo, Nb, Pb, V and Gd intermediate affinities. The elements with inorganic affinities are Al, Si, K, P, Be, Cr, Cs, Ga, Hf, Ni, Sc, Sn, Sr, Ta, Th, Tl, U, W, Y, Zn, Zr, La, Ce, Pr, Nd, Sm, Eu, Tb, Dy, Ho, Er, Tm, Yb and Lu, and are also associated with aluminosilicates. The elements with sulfur affinities are As, Hg, Sb and Se. The dendrogram obtained for EO (Figure 15) is clearly divided between the elements with organic and intermediate affinities on one side, including the elements with sulfur affinities, and the elements with inorganic affinities belong to the other group, comprising the elements with aluminosilicate affinities and all REE.

4.5. The REE as Proxies of Geochemical Processes

The REE concentrations and their distribution pattern are important indicators of geochemical processes and allow to assess the contribution of depositional and/or epigenetic processes in REE enrichment and/or anomalies (among others, [47,78,82,83]).

Thus, the REE concentrations of the studied samples were normalized to the geochemical composition of the Upper Continental Crust (UCC), using data from Taylor and McLennan [84], dividing the content obtained in the REE elements of the studied sam-

ples by the value reported for the same element in the UCC. The projection of these data, separating them by unit, is presented in Figure 17.

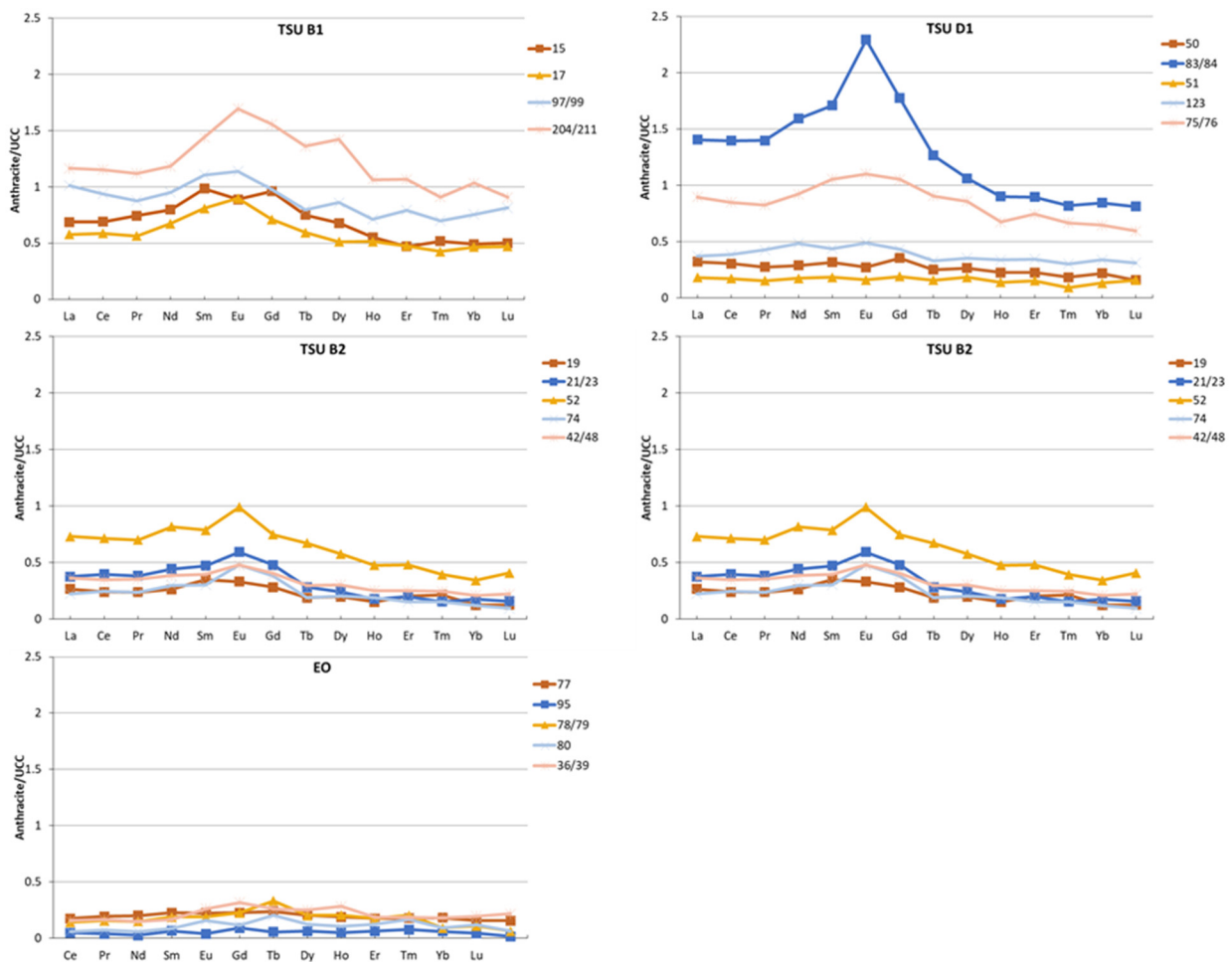


Figure 17. Distribution patterns of REE in the coal samples from TSU and EO. REE are normalized to the Upper Continental Crust (UCC; [84]).

The distribution of the REE in the TSU B1, D1, B2, D2 and the EO samples (Figure 17) shows different patterns. Thus, it is found that some samples are more enriched in REE, particularly in LREE, and a depletion of the elements from the bottom to the top of the sequence is remarkable. It is evident that some samples from TSU B1 and TSU D1 exhibit a slight enrichment in REE and a positive, sometimes quite evident, Eu anomaly [38]. The samples from the EO show no enrichment in REE and their distribution pattern shows a subparallel trend [38]. Thus, the occurrence of REE, in particular the slight enrichment in Eu, appears to be related with different geological processes.

As previously mentioned, in the São Pedro da Cova Coalfield, the occurrence of a granodioritic porphyry [63] between the TSU B1 and TSU D1 was reported [62]. Thus, it is considered that the pattern observed in the EO is associated to the sedimentary contribution, being the more heterogeneous patterns of TSU B1 and TSU D1 associated with the contribution of magmatic fluids [38]. It is also verified that these samples are geographically close (Figure 4), evidencing the local influence of the granodioritic porphyries identified and described in this sector of the DCB by Teixeira and Fonseca [62]. This is supported by other case studies [53,54] which consider that the action of hydrothermal fluids of epigenetic origin contributes to the enrichment of REE [85].

4.6. Mineralogical Evidence of Magmatic Fluids

Mercury has high affinities for organic carbon as well as sulfide, namely pyrite, e.g., [55,56,86,87]. In the São Pedro da Cova Coalfield, Hg displays an intermediate affinity with ash yield ($r_{\text{Ash-Hg}} = 0.03$) and a sulfur affinity ($r_{\text{S tot-Hg}} = 0.64$), considering all studied samples. The intermediate affinity may indicate both an organic and inorganic association of Hg in the studied coals. However, considering the samples from TSU B1, where the samples are extremely enriched, this element has an organic association ($r_{\text{Ash-Hg}} = -0.90$) and a strong sulfur affinity ($r_{\text{S tot-Hg}} = 0.71$). This positive affinity with S tot points to an association with sulfide minerals. As mentioned before, SEM-EDS analysis revealed the occurrence of cinnabar (HgS, Figure 15). This Hg sulfide occurs, frequently, in particles of about 50 μm in size. Pyrite, which is considered as the main carrier of Hg in coals [55], was observed both in framboidal form and filling cleats, but the occurrence of Hg was not identified neither in pyrite nor in organic matter. The cinnabar mineralization is clearly of epigenetic origin as sometimes cinnabar appears filling devolatilization vacuoles in coal. These devolatilization vacuoles are the result of significant thermal effects and reflect the high degree of pressure and temperature reached during the coalification process. This mineralization is thus clearly subsequent to the coal formation and its thermal alteration. This is also supported by Brownfield et al. [86], who reported cinnabar in Franklin No. 7–8–9 coal samples and stated that higher Hg content in coals is associated with hydrothermal mineralization ([86,87] and references therein).

The primary factors of Hg enrichment in coal deposits are intrusion of low-temperature hydrothermal fluids and magmatic-hydrothermal fluids [54,55,86,87]. As mentioned before, a porphyry intrusion was observed inside of the São Pedro da Cova Coalfield [62], immediately at the top of TSU B1; therefore, since coal samples from this unit show the highest Hg contents, this may be associated with the unusual enrichment in Hg observed in the coal sample from this area. The occurrence of cinnabar was previously reported in this area of the DCB by Moura et al. [37] and considered to be epigenetic in nature as it fills devolatilization vacuoles resulting from the action of Hg-enriched hydrothermal fluids that acted at depth [37].

The occurrence of alumino-phosphates (goyazite-gorceixite minerals) is considered as an indicator of volcanic input ([59] and references therein). Although the P content of the studied samples was low, showing a depletion in all studied samples (Figure 13), a barium alumino-phosphate, gorceixite, was identified (Figure 12). The occurrence of this mineral is also clearly epigenetic, as it occurs filling devolatilization pores in the organic matter (Figure 12).

The mode of occurrence of the Ba is, beyond other minerals, gorceixite and barite [56], both identified in the studied samples. In addition to the gorceixite, as mentioned before, other phosphates were observed, namely xenotime (Y phosphate, containing Dy and Gd), monazite (Ce phosphate with La and Nd) and fluorapatite, the most common, that have, in some cases, also an epigenetic origin. Considering the correlation coefficient between P and the main elements of the phosphates identified, Ca, Ba, Ce and Y, it is noticed that for TSU B1 and D1 the correlation coefficients are clearly high ($r_{\text{P-element}} > 0.74$, except for Ca of TSU D1) while the lower values were found for the EO.

The occurrence of both cinnabar and gorceixite in the studied samples reveal a volcanic input and take into account that a vein of porphyry intrusion was identified between the TSU B1 and TSU D1; it is suggested that an epigenetic mineralization was responsible for the enrichment of the majority of the elements quantified in the samples of this sedimentary sequence as well as the different patterns of the REE. Furthermore, the general depletion of the elements observed in the EO, the subparallel distribution pattern of the REE, and the low correlation coefficients observed between P and the elements of the phosphate identified in the samples suggest that their geochemical composition is associated with the sedimentary contribution. In this context, it can be stated that the tectonic slicing of the EO occurred previously to the epigenetic mineralization.

In addition to the mineralogical evidence of an epigenetic mineralization, pyrolytic carbon was identified in these coals [21]. Pyrolytic carbon was found in coals that suffered thermal events during the deformation stages, such as folding and faulting of coal seams ([88], and references therein). Thus, the occurrence of this organic component suggests, and is in accordance, with the influence of magmatic fluids related to the intrusion of the porphyry vein as well as the tectonic context previously described for the DCB.

5. Conclusions

In this study the maceral composition and vitrinite reflectance were determined and the major and trace element compositions were analyzed to characterize the organic matter of coals from the DCB, and to identify the mode of occurrence of the elements and their enrichment/depletion considering the values established for the worldwide hard coals. The obtained results can be outlined as follows:

1. The coals from the São Pedro da Cova Coalfield have vitrinite as the main organic component while inertinite also occurs. These coals are classified as anthracite A ($R_r = 4.51\%$ and 5.76%). Ash yield ranges between 4.86% and 39.72% (dry basis). Volatile matter, C and H contents agree with the rank of these coals, while S tot contents are low.
2. In all units, most of the elements as well as REE have inorganic affinities and are associated with the aluminosilicates, with the other elements having affinities with the sulfides. Illite and muscovite are the main phyllosilicates identified by SEM-EDX, and within the sulfides pyrite is the most common, having a syngenetic and epigenetic origin; however, galena, sphalerite, chalcopyrite and cinnabar were also identified.
3. The trace element concentration coefficients indicate that TSU 1 has more elements that demonstrate enrichment, especially As, Cs and Hg, the last one being extremely enriched. The EO shows a depletion in almost all elements. Regarding the geochemical affinities, Hg presents an intermediate affinity with the ash yield and a positive affinity with S tot, indicating that it occurs as a sulfide. Cinnabar was identified filling devolatilization vacuoles in the coal.
4. The different REE distribution patterns observed in the TSU B1, D1, B2 and D2 samples, and a general enrichment of most of the quantified elements, namely LREE, are considered to be associated with magmatic fluid contribution, while for the EO a subparallel trend of the REE distribution patterns, a depletion of REE and of the other elements in general, are considered to be related to the sedimentary contribution.
5. The samples are geographically close together evidencing the local influence of the granodioritic porphyry identified and described only in this sector of the DCB. Despite the low content of P in the studied samples, gorceixite (Ba aluminophosphate) was identified as having an epigenetic origin, occurring filling devolatilization pores in the organic matter. Other REE-phosphates such as monazite and xenotime were also identified.
6. The cinnabar and gorceixite mineralization are of epigenetic origin and may result from the action of a porphyry intrusion identified in this area of the DCB between the TSU B1 and TSU D1.

Supplementary Materials: The following are available online at <https://www.mdpi.com/article/10.3390/min12020275/s1>, Table S1: Sample reference and location; Table S2: Petrographic composition (maceral analysis) and random vitrinite reflectance (%R_r); proximate and ultimate analyses data; and major and trace element composition of the studied coals.

Author Contributions: Conceptualization, D.F.; methodology, M.C., H.M. and I.S.-R.; investigation, M.C. and H.M.; resources, D.F.; writing—original draft preparation, D.F., A.P.d.J. and M.C.; writing—review and editing, D.F., A.P.d.J., M.C. and I.S.-R.; supervision, D.F. and A.P.d.J. All authors have read and agreed to the published version of the manuscript.

Funding: This research was partially supported by national funds through FCT, projects UIDB/04683/2020 and UIDP/04683/2020.

Informed Consent Statement: Not applicable.

Data Availability Statement: Not applicable.

Acknowledgments: The author H. Moura benefited from a doctoral scholarship financed by the FCT—Fundação para a Ciência e a Tecnologia (Ref: SFRH/BD/ 134109/2017). A special acknowledgement is given to Carolina Fonseca for the support with English editing.

Conflicts of Interest: The authors declare no conflict of interest.

References

1. Domingos, L.C.F.G.; Freire, J.L.S.; Silva, F.G.; Gonçalves, F.; Pereira, E.; Ribeiro, A. The structure of the intramontane Upper Carboniferous basins in Portugal. In *The Carboniferous of Portugal*; Lemos de Sousa, M.J., Oliveira, J.T., Eds.; Memórias dos Serviços Geológicos de Portugal: Lisboa, Portugal, 1983; Volume 29, pp. 187–194.
2. Ribeiro, A.; Rodrigues, J.F.; Pinto de Jesus, A.; Pereira, E.; Lemos de Sousa, M.J.; Brandão Silva, J. Novos Dados sobre a Estratigrafia e Estrutura da Zona de Cisalhamento do Sulco Carbonífero Dúrico-Beirão. In *Evolução Geológica do Maciço Ibérico e seu Enquadramento Continental*; Reunião Anual do PICG-376-Laurentia-Gondwana-Báltica Connections; Comunicações XIV Reunião de Geologia do Oeste Peninsular; Pires, C.C., Gomes, M.E.P., Coke, C., Eds.; UTAD: Vila Real, Portugal, 1983; pp. 195–201.
3. Pinto de Jesus, A. Gênese e Evolução da Bacia Carbonífera do Douro (Estefaniano C inferior, NW de Portugal); Um Modelo. Ph.D. Thesis, University of Porto, Porto, Portugal, 2001.
4. Pinto de Jesus, A. Evolução sedimentar e tectónica da Bacia Carbonífera do Douro (Estefaniano C inferior, NW de Portugal). *Cad. Geol. Laxe* **2003**, *28*, 107–125.
5. Pinto de Jesus, A. Carboniferous Intermontane Basins of Portugal. In *The Geology of Iberia: A Geodynamic Approach*, 1st ed.; Oliveira, J., Quesada, C., Eds.; Springer Nature Switzerland AG: Cham, Switzerland, 2019; Synorogenic Basins; Volume 2, pp. 402–408.
6. Teixeira, C. O Antracólítico Continental Português (Estratigrafia e Tectónica). Ph.D. Thesis, University of Porto, Porto, Portugal, 1944.
7. Teixeira, C. O Sistema Permo-Carbónico. In *Notas sobre Geologia de Portugal*; Lisboa, Portugal, 1954.
8. Wagner, R.H.; Lemos de Sousa, M.J. The Carboniferous Megaflores of Portugal—A revision of identifications and discussion of stratigraphic ages. In *The Carboniferous of Portugal*; Lemos de Sousa, M.J., Oliveira, J.T., Eds.; Memórias dos Serviços Geológicos de Portugal: Lisboa, Portugal, 1983; Volume 29, pp. 127–152.
9. Correia, P.; Šimůnek, Z.; Pšenička, J.; Sá, A.A.; Domingos, R.; Carneiro, A.; Flores, D. New paleobotanical data on the Portuguese Pennsylvanian (Douro Carboniferous Basin, NW Portugal). *Commun. Geol.* **2014**, *101*, 409–414.
10. Correia, P.; Sá, A.A.; Murphy, J.B.; Šimůnek, Z.; Flores, D. *Lesleya* Lesquereux from the Pennsylvanian of the Iberian Massif: Part of a dryland megaflores from the Variscan orogen, northwestern Portugal. *Can. J. Earth Sci.* **2016**, *53*, 883–895. [[CrossRef](#)]
11. Correia, P.; Šimůnek, Z.; Artur, S.A.; Flores, D. A new Late Pennsylvanian floral assemblage from the Douro Basin, Portugal. *Geol. J.* **2018**, *53*, 2507–2531. [[CrossRef](#)]
12. Correia, P.; Šimůnek, Z.; Cleal, C.; Sá, A. *Douropteris alvarezii* gen. nov., sp. nov., a new medullosalean pteridosperm from the Late Pennsylvanian of Portugal. *Geol. J.* **2019**, *54*, 1567–1577. [[CrossRef](#)]
13. Eagar, R.M.C. The non-marine bivalve fauna of the Stephanian C of North Portugal. In *The Carboniferous of Portugal*; Lemos de Sousa, M.J., Oliveira, J.T., Eds.; Memórias dos Serviços Geológicos de Portugal: Lisboa, Portugal, 1983; Volume 29, pp. 179–185.
14. Loureiro, J.P.; Correia, P.; Nel, A.; Pinto de Jesus, A. *Lusitaneura covensis* n. gen., n. sp., first Caloneurodeia from the Carboniferous of Portugal (Insecta: Pterygota: Panorthoptera). *An. Soc. Entomol. Fr.* **2010**, *46*, 242–246. [[CrossRef](#)]
15. Correia, P.; Murphy, J.B.; Sá, A.A.; Domingos, R.; Flores, D. First Palaeozoic arachnid from Portugal and implications for Carboniferous palaeobiogeography. *Geol. J.* **2013**, *48*, 101–107. [[CrossRef](#)]
16. Correia, P.; Nel, A.; Sá, A.A.; Domingos, R.; Carneiro, A.; Flores, D. A new Palaeodictyoptera from the Late Carboniferous of Portugal. *Ann. Soc. Entomol. Fr.* **2013**, *49*, 398–401. [[CrossRef](#)]
17. Lemos de Sousa, M.J. Contribuição para o Conhecimento da Bacia Carbonífera do Douro. Ph.D. Thesis, University of Porto, Porto, Portugal, 1973.
18. Lemos de Sousa, M.J. Novos elementos para o conhecimento da relação “Microdureza Vickers-Rang” em carvões. (A propósito das primeiras determinações de microdureza em carvões portugueses). *Publ. Mus. Labor. Miner. Geol. Fac. Ciênc. Porto* **1976**, *86*, 69.
19. Lemos de Sousa, M.J. Nota sobre a densidade das perantracites da bacia carbonífera do Douro (NW) de Portugal. *Bol. Min.* **1977**, *14*, 1–7.
20. Lemos de Sousa, M.J. Sobre alguns problemas do Permo-carbónico continental português. *Ciênc. Terra* **1977**, *3*, 9–22.
21. Lemos de Sousa, M.J. *Contribution à l'étude du Bassin Houiller du Douro (NW du Portugal)*. *Atlas de Micropétrographie des Peranthracites*; Direcção-Geral de Geologia e Minas, Serviços Geológicos de Portugal: Lisboa, Portugal, 1978; Volume 26, 92p.
22. Lemos de Sousa, M.J. O grau de incarbonização (rang) dos carvões durienses e as consequências genéticas, geológicas e estruturais que resultam do seu conhecimento. *Commun. Serv. Geol. Portg.* **1978**, *63*, 179–365.
23. Lemos de Sousa, M.J. Subsídios para o conhecimento da matéria mineral associada às perantracites da bacia carbonífera do Douro (NO Portugal). I—Um plano de pesquisa. *Commun. Serv. geol. Portg.* **1979**, *64*, 81–98.

24. Lemos de Sousa, M.J. Subsídios para o conhecimento da matéria mineral associada às perantracites da bacia carbonífera do Douro (NO Portugal). II—Elementos para o estudo geoquímico das perantracites durienses. *Comun. Serv. geol. Portg.* **1979**, *64*, 99–102.
25. Marques, M.; Suárez-Ruiz, I.; Flores, D.; Guedes, A.; Rodrigues, S. Correlation between optical, chemical and micro-structural parameters of high-rank coals and graphite. *Int. J. Coal Geol.* **2009**, *77*, 377–382. [[CrossRef](#)]
26. Ribeiro, J.; Ferreira da Silva, E.; Flores, D. Burning of coal waste piles from Douro Coalfield (Portugal): Petrological, geochemical and mineralogical characterization. *Int. J. Coal Geol.* **2010**, *81*, 359–372. [[CrossRef](#)]
27. Ribeiro, J.; Ferreira da Silva, E.; Pinto de Jesus, A.; Flores, D. Petrographic and geochemical characterization of coal waste piles from Douro Coalfield (NW Portugal). *Int. J. Coal Geol.* **2011**, *87*, 226–236. [[CrossRef](#)]
28. Ribeiro, J.; Moura, R.; Flores, D.; Lopes, D.B.; Gouveia, C.; Mendonça, S.; Frazão, O. The Douro Coalfield Fires of Portugal. In *Coal and Peat Fires: A Global Perspective*; Stracher, G.B., Prakash, A., Sokol, E.V., Eds.; Elsevier: Amsterdam, The Netherlands, 2013; Volume II, pp. 314–337.
29. Ribeiro, J.; Viveiros, D.; Ferreira, J.; Santos, J.L.; Baptista, J.M.; Flores, D. Monitorização ambiental de escombreira de S. Pedro da Cova: Temperatura de combustão. *Comun. Geol.* **2014**, *101*, 1063–1065.
30. Ribeiro, J.; Sant’Ovaia, H.; Gomes, C.; Ward, C.; Flores, D. Mineralogy and Magnetic Parameters of Materials from the Douro Coalfield, Northwest of Portugal. In *Coal and Peat Fires: A Global Perspective*; Stracher, G.B., Prakash, A., Sokol, E.V., Eds.; Elsevier: Amsterdam, The Netherlands, 2015; Volume III, pp. 494–508.
31. Ribeiro, J.; Viveiros, D.; Ferreira, J.; Lopez-Gil, A.; Dominguez-Lopez, A.; Martins, H.F.; Perez-Herrera, R.; Lopez-Aldaba, A.; Duarte, L.; Pinto, A.; et al. ECOAL project-Delivering Solutions for Integrated monitoring of coal-related fires supported on optical fiber sensing technology. *Appl. Sci.* **2017**, *7*, 956. [[CrossRef](#)]
32. Rocha, J.; Santos, P.; Ribeiro, J.; Espinha Marques, J.; Mansilha, C.; Flores, D. Caracterização hidrogeoquímica de efluentes da mina de carvão de São Pedro da Cova (Gondomar). *Comun. Geol.* **2020**, *107*, 129–132.
33. Santos, P.; Espinha Marques, J.; Ribeiro, J.; Rocha, J.; Flores, D. Caracterização da Contaminação dos Solos da Envolvente da Escombreira da Antiga Mina de Carvão de São Pedro da Cova. *Comun. Geol.* **2020**, *107*, 151–154.
34. Teodoro, A.; Santos, P.; Espinha Marques, J.; Ribeiro, J.; Mansilha, C.; Melo, A.; Duarte, L.; Rodrigues de Almeida, C.; Flores, D. An Integrated Multi-Approach to Environmental Monitoring of a Self-Burning Coal Waste Pile: The São Pedro da Cova Mine (Porto, Portugal) Study Case. *Environments* **2021**, *8*, 48. [[CrossRef](#)]
35. Espinha Marques, J.; Martins, V.; Santos, P.; Ribeiro, J.; Mansilha, C.; Melo, A.; Rocha, F.; Flores, D. Changes Induced by Self-Burning in Technosols from a Coal Mine Waste Pile: A Hydroopedological Approach. *Geosciences* **2021**, *11*, 195. [[CrossRef](#)]
36. Mansilha, C.; Melo, A.; Flores, D.; Ribeiro, J.; Rocha, J.R.; Martins, V.; Santos, P.; Espinha Marques, J. Irrigation with Coal Mining Effluents: Sustainability and Water Quality Considerations (São Pedro da Cova, North Portugal). *Water* **2021**, *13*, 2157. [[CrossRef](#)]
37. Moura, H.; Pinto de Jesus, A.D.; Ribeiro, J.; Suárez-Ruiz, I.; Flores, D.; Cunha, P.P. Occurrence of Mercury and enrichment source in coals from the Douro Carboniferous Basin, São Pedro da Cova area (NW Portugal). In Proceedings of the 70th Annual Meeting of the International Committee for Coal and Organic Petrology, Brisbane, Australia, 23–29 September 2018; pp. 71–72.
38. Costa, M.; Moura, H.; Pinto de Jesus, A.D.; Flores, D. Assinatura geoquímica de fluídos ígneos nos carvões da Bacia Carbonífera do Douro: Sector de São Pedro da Cova. In *Jornadas ICT 2021, Porto*; Livro de Resumos; Instituto de Ciências da Terra: Porto, Portugal, 2021; pp. 43–44.
39. Goodarzi, F.; Gentzis, T.; Bustin, R.M. Reflectance and petrology profile of a partially combusted and coked bituminous coal seam from British Columbia. *Fuel* **1988**, *67*, 1218–1222. [[CrossRef](#)]
40. Goodarzi, F.; Cameron, A.R. Organic Petrology and Elemental Distribution in Thermally Altered Coals from Telkwa, British Columbia. *Energy Sources* **1990**, *12*, 315–343. [[CrossRef](#)]
41. Finkelman, R.B.; Bostick, N.H.; Dulong, F.T.; Senftle, F.E.; Thorpe, A.N. Influence of an igneous intrusion on the inorganic geochemistry of a bituminous coal from Pitkin County, Colorado. *Int. J. Coal Geol.* **1998**, *36*, 223–241. [[CrossRef](#)]
42. Dai, S.; Ren, D. Effects of magmatic intrusion on mineralogy and geochemistry of coals from the Fengfeng–Handan Coalfield, Hebei, China. *Energy Fuel* **2007**, *21*, 1663–1673. [[CrossRef](#)]
43. Golab, A.N.; Hutton, A.C.; French, D. Petrography, carbonate mineralogy and geochemistry of thermally altered coal in Permian coal measures, Hunter Valley, Australia. *Int. J. Coal Geol.* **2007**, *70*, 150–165. [[CrossRef](#)]
44. Colmenero, J.R.; Suárez-Ruiz, I.; Fernández-Suárez, J.; Barba, P.; Llorens, T. Genesis and rank distribution of Upper Carboniferous coal basins in the Cantabrian Mountains, Northern Spain. *Int. J. Coal Geol.* **2008**, *76*, 187–204. [[CrossRef](#)]
45. Goodarzi, F.; Gentzis, T.; Dewing, K. Influence of igneous intrusions on the thermal maturity of organic matter in the Sverdrup Basin, Arctic Canada. *Int. J. Coal Geol.* **2019**, *213*, 103280. [[CrossRef](#)]
46. Rodrigues, S.; Esterle, J.; Ward, V.; Glasser, L.; Maquissene, T.; Etchart, E. Flow structures and mineralisation in thermally altered coal from the Moatize Basin, Mozambique. *Int. J. Coal Geol.* **2020**, *228*, 103551. [[CrossRef](#)]
47. Moura, H.; Suárez-Ruiz, I.; Marques, M.M.; Ribeiro, J.; Cunha, P.P.; Flores, D. Influence of magmatic fluids on the organic and inorganic fractions of coals from the Peñarroya-Belmez-Espiel Basin (Spain). *Int. J. Coal Geol.* **2021**, *235*, 103679. [[CrossRef](#)]
48. Dai, S.; Ren, D.; Chou, C.-L.; Finkelman, R.B.; Seredin, V.V.; Zhou, Y. Geochemistry of trace elements in Chinese coals: A review of abundances, genetic types, impacts on human health, and industrial utilization. *Int. J. Coal Geol.* **2012**, *94*, 3–21. [[CrossRef](#)]
49. Yan, Z.; Liu, G.; Sun, R.; Wu, D.; Wu, B.; Zhou, C. Mercury distribution in coals influenced by magmatic intrusions, and surface waters from the Huaibei Coal Mining District, Anhui, China. *Appl. Geochem.* **2013**, *33*, 298–305. [[CrossRef](#)]

50. Chen, J.; Liu, G.; Li, H.; Wu, B. Mineralogical and geochemical responses of coal to igneous intrusion in the Pansan Coal Mine of the Huainan coalfield, Anhui, China. *Int. J. Coal Geol.* **2014**, *124*, 11–35. [[CrossRef](#)]
51. An, Y.; Liu, L.; Wang, M.; Zheng, S.; Guo, Y.; Zhang, S.; Lai, C. Source and Enrichment of toxic elements in Coal Seams around Mafic Intrusions: Constraints from Pyrites in the Yuandian Coal Mine in Anhui, Eastern China. *Minerals* **2018**, *8*, 164. [[CrossRef](#)]
52. Zheng, L.; Liu, G.; Chou, C.L. Abundance and modes of occurrence of mercury in some low-sulfur coals from China. *Int. J. Coal Geol.* **2008**, *73*, 19–26. [[CrossRef](#)]
53. Dai, S.; Zhang, W.; Ward, C.R.; Seredin, V.V.; Hower, J.C.; Li, X.; Song, W.; Wang, X.; Kang, H.; Zheng, L.; et al. Mineralogical and geochemical anomalies of late Permian coals from the Fusui Coalfield, Guangxi Province, southern China: Influences of terrigenous materials and hydrothermal fluids. *Int. J. Coal Geol.* **2013**, *105*, 60–84. [[CrossRef](#)]
54. Dai, S.; Li, T.; Jiang, Y.; Ward, C.R.; Hower, J.C.; Sun, J.; Liu, J.; Song, H.; Wei, J.; Li, Q.; et al. Mineralogical and geochemical compositions of the Pennsylvanian coal in the Hailiushu Mine, Daqingshan Coalfield, Inner Mongolia, China: Implications of sediment-source region and acid hydrothermal solutions. *Int. J. Coal Geol.* **2015**, *137*, 92–110. [[CrossRef](#)]
55. Yudovich, Y.E.; Ketris, M.P. Mercury in coal: A review: Part 1. Geochemistry. *Int. J. Coal Geol.* **2005**, *62*, 107–134. [[CrossRef](#)]
56. Finkelman, R.B.; Shifeng, D.; French, D. The importance of minerals in coal as the hosts of chemical elements: A review. *Int. J. Coal Geol.* **2019**, *212*, 103251. [[CrossRef](#)]
57. Ward, C.R.; Corcoran, J.F.; Saxby, J.D.; Read, H.W. Occurrence of phosphorus minerals in Australian coal seams. *Int. J. Coal Geol.* **1996**, *30*, 185–210. [[CrossRef](#)]
58. Dai, S.; Zou, J.; Jiang, Y.; Ward, C.R.; Wang, X.; Li, T.; Xue, W.; Liu, S.; Tian, H.; Sun, X.; et al. Mineralogical and geochemical compositions of the Pennsylvanian coal in the Adaohai Mine, Daqingshan Coalfield, Inner Mongolia, China: Modes of occurrence and origin of diasporite, gorceixite and ammonian illite. *Int. J. Coal Geol.* **2012**, *194*, 250–2740. [[CrossRef](#)]
59. Dai, S.; Hower, J.C.; Ward, C.R.; Guo, W.; Song, H.; O’Keefe, J.M.K.; Xie, P.; Hood, M.M.; Yan, X. Elements and phosphorous minerals in the middle Jurassic inertinite-rich coals of the Muli Coalfield on the Tibetan Plateau. *Int. J. Coal Geol.* **2015**, *144–145*, 23–47. [[CrossRef](#)]
60. Goodarzi, F.; Grieves, D.A.; Labonté, M. Mineralogical and elemental composition of Tonsteins from the East Kootenay Coalfields, Southeastern British Columbia. *Energy Sources* **1990**, *12*, 265–295. [[CrossRef](#)]
61. Goodarzi, F.; Van der Flier-Keller, E. Organic petrology and geochemistry of intermontane coals from British Columbia, III. The Blakeburn opencast mine near Tulameen, British Columbia, Canada. *Chem. Geol.* **1989**, *75*, 227–247. [[CrossRef](#)]
62. Teixeira, C.; Fonseca, N. Formações eruptivas relacionadas com o Estefaniano de São Pedro da Cova. In *Anais da Faculdade de Ciências da Universidade do Porto, Tomo XXX*; Imprensa Portuguesa: Porto, Portugal, 1945; pp. 100–109.
63. Pereira, J. Estudo petrográfico de rochas porfíricas de São Pedro da Cova. In *Anais da Faculdade de Ciências da Universidade do Porto, Tomo XXX*; Imprensa Portuguesa: Porto, Portugal, 1945; pp. 116–136.
64. Pinto de Jesus, A.; Lemos de Sousa, M.J. Modelo deposicional da Bacia Carbonífera do Douro na região de Sete Casais (Sector NW do Sulco Carbonífero Dúrico-Beirão). In *Actas do V Congresso Nacional de Geologia (Resumos Alargados)*; Comunicações do Instituto Geológico Mineiro, Volume 84; Instituto Geológico Mineiro: Lisboa, Portugal, 1998; Volume 1, pp. A22–A25.
65. Megias, A.G. Introducción al análisis tectosedimentario: Aplicación al estudio dinámico de cuencas. In *Actas Congreso Latinoamericano de Geología, Argentina*; Serviço Geológico Nacional: Buenos Aires, Argentina, 1982; Volume I, pp. 385–401.
66. ISO 7404–3; *Methods for the Petrographic Analysis of Coals—Part 3: Method of Determining Maceral Group Composition*. International Organization for Standardization: Geneva, Switzerland, 2009; 7p.
67. ISO 7404–5; *Methods for the Petrographic Analysis of Coals—Part 5: Method of Determining Microscopically the Reflectance of Vitrinite*. International Organization for Standardization: Geneva, Switzerland, 2009; 14p.
68. ISO 7404–2; *Methods for the Petrographic Analysis of Coals—Part 2: Methods of Preparing Coal Samples*. International Organization for Standardization: Geneva, Switzerland, 2009; 12p.
69. International Committee for Coal and Organic Petrology (ICCP). The new vitrinite classification (ICCP System 1994). *Fuel* **1998**, *77*, 349–358. [[CrossRef](#)]
70. International Committee for Coal and Organic Petrology (ICCP). The new inertinite classification (ICCP System 1994). *Fuel* **2001**, *80*, 459–471. [[CrossRef](#)]
71. ISO 562; *Hard Coal and Coke—Determination of Volatile Matter*. International Organization for Standardization: Geneva, Switzerland, 2010; 7p.
72. ISO 589; *Hard Coal—Determination of Total Moisture*. International Organization for Standardization: Geneva, Switzerland, 2008; 9p.
73. ISO 1171; *Solid Mineral Fuels—Determination of Ash*. International Organization for Standardization: Geneva, Switzerland, 2010; 4p.
74. ISO 1170; *Coal and Coke—Calculation of Analyses to Different Bases*. International Organization for Standardization: Geneva, Switzerland, 2013; 7p.
75. ISO 11760; *Classification of Coals*. 1st ed. International Organization for Standardization: Geneva, Switzerland, 2005; 9p.
76. Taylor, G.H.; Teichmüller, M.; Davis, A.; Diessel, C.F.K.; Littke, R.; Robert, P. *Organic Petrology*; Gerbrüder Borntraeger: Berlin/Stuttgart, Germany, 1998; 704p.
77. Ketris, M.P.; Yudovich, Y.E. Estimations of Clarkes for Carbonaceous biolithes: World averages for trace element contents in black shales and coals. *Int. J. Coal Geol.* **2009**, *78*, 135–148. [[CrossRef](#)]

78. Dai, S.; Seredin, V.V.; Ward, C.R.; Hower, J.C.; Xing, Y.; Zhang, W.; Song, W.; Wang, P. Enrichment of U-Se-Mo-Re-V in coals preserved within marine carbonate successions: Geochemical and mineralogical data from the late Permian Guiding Coalfield, Guizhou, China. *Miner. Depos.* **2015**, *50*, 159–186. [[CrossRef](#)]
79. Dai, S.; Chekryzhov, I.Y.; Seredin, V.V.; Nechaev, V.P.; Graham, I.T.; Hower, J.C.; Ward, C.R.; Ren, D.; Wang, X. Metalliferous coal deposits in East Asia (Primorye of Russia and South China): A review of geodynamic controls and styles of mineralization. *Gondwana Res.* **2016**, *29*, 60–82. [[CrossRef](#)]
80. Finkelman, R.B.; Palmer, C.A.; Wang, P. Quantification of the modes of occurrence of 42 elements in coal. *Int. J. Coal Geol.* **2018**, *185*, 138–160. [[CrossRef](#)]
81. Couto, H. As Mineralizações de Sb-Au da Região Dúrico-Beirã. Ph.D. Thesis, University of Porto, Porto, Portugal, 1993.
82. Dai, S.; Graham, I.T.; Ward, C.R. A review of anomalous rare earth elements and yttrium in coal. *Int. J. Coal Geol.* **2016**, *159*, 82–95. [[CrossRef](#)]
83. Zhao, L.; Dai, S.; Nechaev, V.P.; Nechaeva, E.V.; Graham, I.T.; French, D.; Sun, J. Enrichment of critical elements (Nb-Ta-Zr-Hf-REE) within coal and host rocks from the Datanhao mine, Daqingshan Coalfield, northern China. *Ore Geol. Rev.* **2019**, *111*, 102951. [[CrossRef](#)]
84. Taylor, S.R.; McLennan, S.M. *The Continental Crust; Its Composition and Evolution; An Examination of the Geochemical Record Preserved in Sedimentary Rocks*; Blackwell: Oxford, UK, 1985; 312p.
85. Seredin, V.V.; Dai, S. Coal deposits as potential alternative sources for lanthanides and yttrium. *Int. J. Coal Geol.* **2012**, *94*, 67–93. [[CrossRef](#)]
86. Brownfield, M.E.; Affolter, R.H.; Cathcart, J.D.; Johnson, S.Y.; Brownfield, I.K.; Rice, C.A. Geologic setting and characterization of coals and the modes of occurrence of selected elements from the Franklin coal zone, Puget Group, John Henry No. 1 mine, King County, Washington, USA. *Int. J. Coal Geol.* **2005**, *63*, 247–275. [[CrossRef](#)]
87. Dai, S.; Finkelman, R.B.; French, D.; Hower, J.C.; Graham, I.T.; Zhao, F. Modes of occurrence of elements in coal: A critical evaluation. *Earth Sci. Rev.* **2021**, *222*, 103815. [[CrossRef](#)]
88. Kwiecińska, B.; Pusz, S. Pyrolytic carbon—Definition, classification and occurrence. *Int. J. Coal Geol.* **2016**, *163*, 1–7. [[CrossRef](#)]